Obrabotka metallov (tekhnologiya, oborudovanie, instrumenty) = Metal Working and Material Science. 2026 vol. 28 no. 1 pp. 253–261
ISSN: 1994-6309 (print) / 2541-819X (online)
DOI: 10.17212/1994-6309-2026-28.1-253-261

NSTU NETI

Obrabotka metallov -
Metal Working and Material Science

Journal homepage: http://journals.nstu.ru/obrabotka_metallov

Microstructure and mechanical properties of Ti-6Al-4V: a comparison between selective laser melting, electron beam melting, and spark plasma sintering

Javad Karimi *

Technische Universität Bergakademie Freiberg, 6 Akademiestraße, Freiberg, 09599, Germany

https://orcid.org/0000-0002-2733-206X, javadkarimimr@gmail.com

ARTICLE INFO

Article history:
Received: 26 July 2025
Revised: 11 October 2025
Accepted: 17 December 2025
Available online: 15 March 2026

Keywords:
Titanium alloy
Additive manufacturing
Selective laser melting
Electron beam melting
Spark plasma sintering
Microstructure
Remelting

ABSTRACT

Introduction. *Ti-6Al-4V* is one of the most commonly used α+β titanium alloys in various industries due to its excellent specific strength and corrosion resistance. Additive manufacturing (*AM*) processes enable the production of *Ti-6Al-4V* parts with complex geometries. However, defects and microstructural inhomogeneity in the fabricated parts can adversely affect their mechanical properties. ***Purpose of the work.*** The purpose of this study is to investigate the microstructure and mechanical properties of *Ti-6Al-4V* parts. The defect density and inhomogeneity in the microstructure and mechanical properties of parts fabricated by selective laser melting (*SLM*), electron beam melting (*EBM*), and spark plasma sintering (*SPS*) were examined. The inhomogeneity in mechanical properties, specifically hardness, was quantified. Furthermore, the effects of a laser remelting strategy on microstructural homogeneity were studied. **Research methods.** *Ti-6Al-4V* parts were fabricated using additive manufacturing processes, namely *SLM* and *EBM*. Parts were also produced via the *SPS* method. A laser remelting strategy (scanning each layer three times) was applied during the *SLM* process. The effects of laser remelting on defects, microstructure, and mechanical properties were studied and compared with standard *SLM* (scanning each layer once), *EBM*, and *SPS*. **Results and discussion.** A lamellar α/α′ microstructure was observed in the *SLM* samples, both in the as-built and remelted conditions (denoted as *SLM* and *SLM-RM*, respectively). The hardness of the *SLM* sample (335 HV) was found to be higher than that of the *SPS* sample (305 HV). Application of the remelting strategy in *SLM* led to an increase in hardness and improved its homogeneity. The average size and shape irregularity of porosities in the *SLM* samples were analyzed; it was observed that surface porosity decreased with the implementation of the remelting strategy. Laser remelting significantly influences the performance of the *SLM* process. The results demonstrate that these synthesis processes yield *Ti-6Al-4V* alloys with distinct microstructural and mechanical properties.

For citation: Karimi J. Microstructure and mechanical properties of Ti-6Al-4V: a comparison between selective laser melting, electron beam melting, and spark plasma sintering. *Obrabotka metallov (tekhnologiya, oborudovanie, instrumenty) = Metal Working and Material Science*, 2026, vol. 28, no. 1, pp. 253–261. DOI: 10.17212/1994-6309-2026-28.1-253-261. (In Russian).

Introduction

Ti-6Al-4V is one of the most commonly used **α+β** titanium alloys due to excellent specific strength and corrosion resistance. Additive manufacturing (*AM*) processes can produce *Ti-6Al-4V* parts with complex geometry for various applications used in many industries. Selective laser melting (*SLM*) and electron beam melting (*EBM*) are powder-based *AM* processes that utilize a focused energy beam to fabricate near-net-shaped components with improved functionalities. Previous studies have reported that the microstructure of *Ti-6Al-4V* fabricated via *SLM* and *EBM* consists of the **α/α′** phase [1–4]. Although a considerable volume of literature has reported the advantages of powder-based *AM* [5–8], there are some disadvantages, such as microstructural anisotropy and porosity, which affect the mechanical properties [9–11].

*** Corresponding author**
Karimi Javad, Doctor of Philological Sciences, Researcher
Technische Universität Bergakademie Freiberg,
6 Akademiestraße,
09599, Freiberg, Germany
Tel.: 49 17674167886, **e-mail:** javadkarimimr@gmail.com

Spark plasma sintering (*SPS*) can sinter *Ti-6Al-4V* powder particles with pressure at high temperature and short holding time. The *SPS* process employs pulsed electrical currents to create localized high temperatures on the surface of the powder particles that promote their consolidation. Even though the heating rate of the *SPS* process is high (1,000 °C/min), the cooling rate is low, which affects the microstructure and mechanical properties. *Yan* et al. [12] studied the microstructure of *Ti-6Al-4V* alloys fabricated via *SLM* and *SPS* and reported that the microstructure consisted of the α/α′ phase and the **α**+**β** dual phase, respectively. However, there is little information about the anisotropy of parts produced using *SPS*.

Many works have reported the application of a re-melting strategy for *SLM* (*SLM-RM*) parts to increase density, modify surface quality, and decrease the residual stress level of the fabricated components [13]. *Mercelis* et al. [14] investigated the impact of laser remelting (post-scanning of each layer) during the *SLM* build process on the stress level. *Brodie* et al. [15] applied re-melting to improve material homogeneity and studied its effects on the microstructure and mechanical properties. Despite the progress in the *AM* of *Ti-6Al-4V*, there is little published work on the anisotropy and inhomogeneity in the microstructure of *SLM*, *SLM-RM*, and *EBM* parts.

Therefore, the present study investigates the microstructure and mechanical properties of additively manufactured *Ti-6Al-4V* components using the *SLM* process. The inhomogeneity in microstructural and mechanical properties of the additively manufactured *Ti-6Al-4V* components is studied. ***This work aims*** to investigate the effect of the re-melting strategy on the microstructure and mechanical properties. The obtained results are compared with those fabricated using *EBM* and *SPS*. The results are compared with those obtained using *EBM* and *SPS*.

Experimental methods

Bulk samples were fabricated from gas-atomized *Ti-6Al-4V* powder particles using *SLM*, *EBM*, and *SPS* processes. An *SLM* machine under an argon atmosphere was used to additively manufacture parts with a layer thickness of 25 μm and a hatch distance of 20 μm. During manufacturing, a scanning rotation angle of 72° was chosen. For *SLM-RM* samples, the powder particles were selectively melted, and the remelting strategy was employed twice with the same processing parameters. In other words, each layer was selectively melted three times. *EBM* samples were fabricated using an *EBM* system manufactured by *Arcam*, with an electron beam size of ~200 μm under vacuum at 10^{-3} mbar. The process started with preheating the powder prior to melting. For part fabrication via *SPS*, approximately 10 g of powder particles were loaded into a graphite die with an inner diameter of 20 mm and compacted using an *SPS* machine in a vacuum of $<10^{-3}$ Pa. During the sintering process, a pressure of 50 MPa was applied. The temperature was raised to 1,100 °C and held for 10 min (dwell time).

A *Zeiss* scanning electron microscope (*SEM*) was utilized for microstructural characterization. Surface porosity, as well as the distribution and size of pores, were determined using image analysis in *ImageJ* software via contrast thresholding. Measurements were performed on optical and scanning electron microscopy images. For each condition, approximately 50 measurements were made across multiple images; mean values and standard deviations are presented.

The crystalline structure of the alloy was studied using an X-ray diffractometer (*Bruker*) with a scanning range of 20° < 2θ < 90° and a 0.01° step size along the build direction. The *Scherrer* equation was used to determine the crystallite size, as follows:

$$D = \frac{K\lambda}{\beta \cos\theta},$$

where $\boldsymbol{D}$ is the crystallite size; $\boldsymbol{K}$ is the shape factor; $\boldsymbol{\beta}$ is the full width at half maximum (*FWHM*) of the diffraction peak; $\boldsymbol{\theta}$ is the *Bragg* angle for the peak; $\boldsymbol{\lambda}$ is the wavelength of the X-ray (*Cu K*α, λ = 1.5406 Å).

Lattice parameters were calculated based on *Bragg's* law and the plane spacing equation for the hexagonal structure:

$$\frac{1}{d^2} = \frac{4}{3}\left(\frac{h^2 + hk + k^2}{a^2}\right) + \frac{l^2}{c^2},$$

$$\lambda = 2d \sin \theta,$$

where $\boldsymbol{d}$ is the interplanar spacing; $\boldsymbol{h}$, $\boldsymbol{k}$, and $\boldsymbol{l}$ are *Miller* indices; $\boldsymbol{a}$ and $\boldsymbol{c}$ are the lattice constants.

Hardness was measured using a *Vickers* hardness machine (*INDENTEC*) with a load of 5 kgf and a dwell time of 10 s.

Results and Discussion

Fig. 1 shows the morphology of the powder particles and their size distribution, where it can be observed that the powder exhibits a narrow distribution with D_{10} ~ 30 µm and D_{90} ~ 63 µm, and the diameter of most particles is ≤ 42 µm (D_{50}). From the *SEM* micrograph, it can be observed that the powder particles are spherical in shape, and some satellite particles are also present.

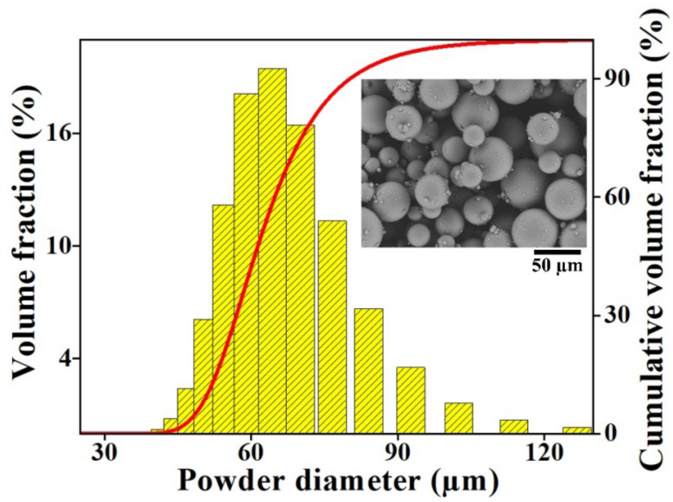

Fig. 1. Histogram of *Ti-6Al-4V* powder particle size distribution (frequency vs. diameter). The average particle size was determined to be 45 ± 14 µm. The inset shows an *SEM* image of the *Ti-6Al-4V* powder particles, revealing a nearly spherical morphology

Fig. 2 shows the X-ray diffraction patterns of *Ti-6Al-4V* gas-atomized powder particles and the bulk *Ti-6Al-4V* samples, including as-*SLM*, *SLM-RM*, *EBM*, and *SPS*. The X-ray diffraction patterns of the samples fabricated via *SLM* show the presence of the **α**/**α′** phase, in agreement with [16–19]. As **α** and **α′** have the same crystalline structure, hexagonal close-packed (*HCP*), and similar lattice parameters, it is difficult to distinguish between the two phases. Similar positions of *XRD* peaks in the range 30–75° were detected between the as-built *SLM* and re-melted samples. However, the presence of weak crystallographic texture is observed between the two patterns. The **α**/**α′** peaks of *SLM* samples are wider than those of *EBM* samples, indicating that *SLM* samples possess a finer **α**/**α′** phase than *EBM* samples. In the *SPS* sample, both *BCC* and *HCP* diffraction peaks were observed, which confirms the existence of **α** and **β** phases. In addition, the effects of the re-melting strategy on the structural data of *SLM* samples, including crystallite size and lattice parameter **α**, were evaluated and compared with those of *EBM* and *SPS* (Table). The crystallite size of the sample fabricated using the *SLM* process was found to be ~17 nm, which is smaller than that of *EBM* and *SPS*.

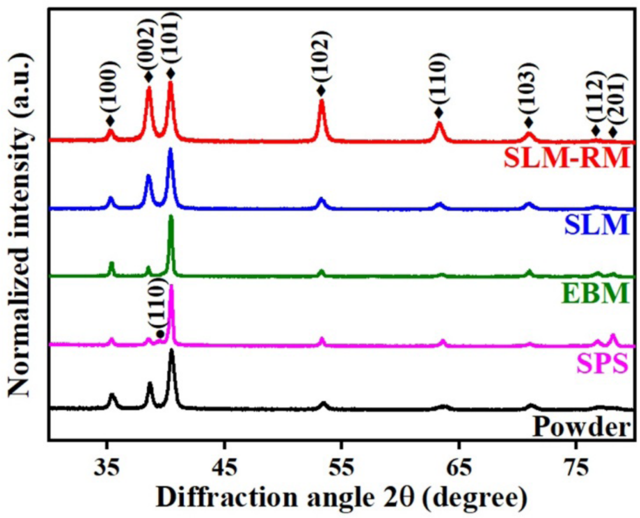

Fig. 2. XRD patterns of *Ti-6Al-4V* powder particles and samples fabricated via *SPS*, *EBM*, *SLM*, and *SLM-RM* processes

Figs. 3, *a–d* show *SEM* images of the *Ti-6Al-4V* samples, where the microstructure of the additively manufactured as-built samples via *SLM*, *SLM-RM*, and *EBM* consists of the **α**/**α′** phase. *Ahmed* et al. [20] investigated the effect of cooling rate on the microstructure of *Ti-6Al-4V* alloys and reported that a cooling rate higher than 410 °C/s results in a fully martensitic microstructure. The cooling rate in *AM* processes,

Crystallite size for the gas-atomized powder and samples fabricated via *SPS*, *EBM*, *SLM*, and *SLM-RM* processes

	Powder	*SPS*	*EBM*	*SLM*	*SLM-RM*
Crystallite size (nm)	16±3	25±5	32±7	18±2	17± 1
Lattice parameter (**α**) (nm)	0.2919	0.2923	0.2925	0.2929	0.2927

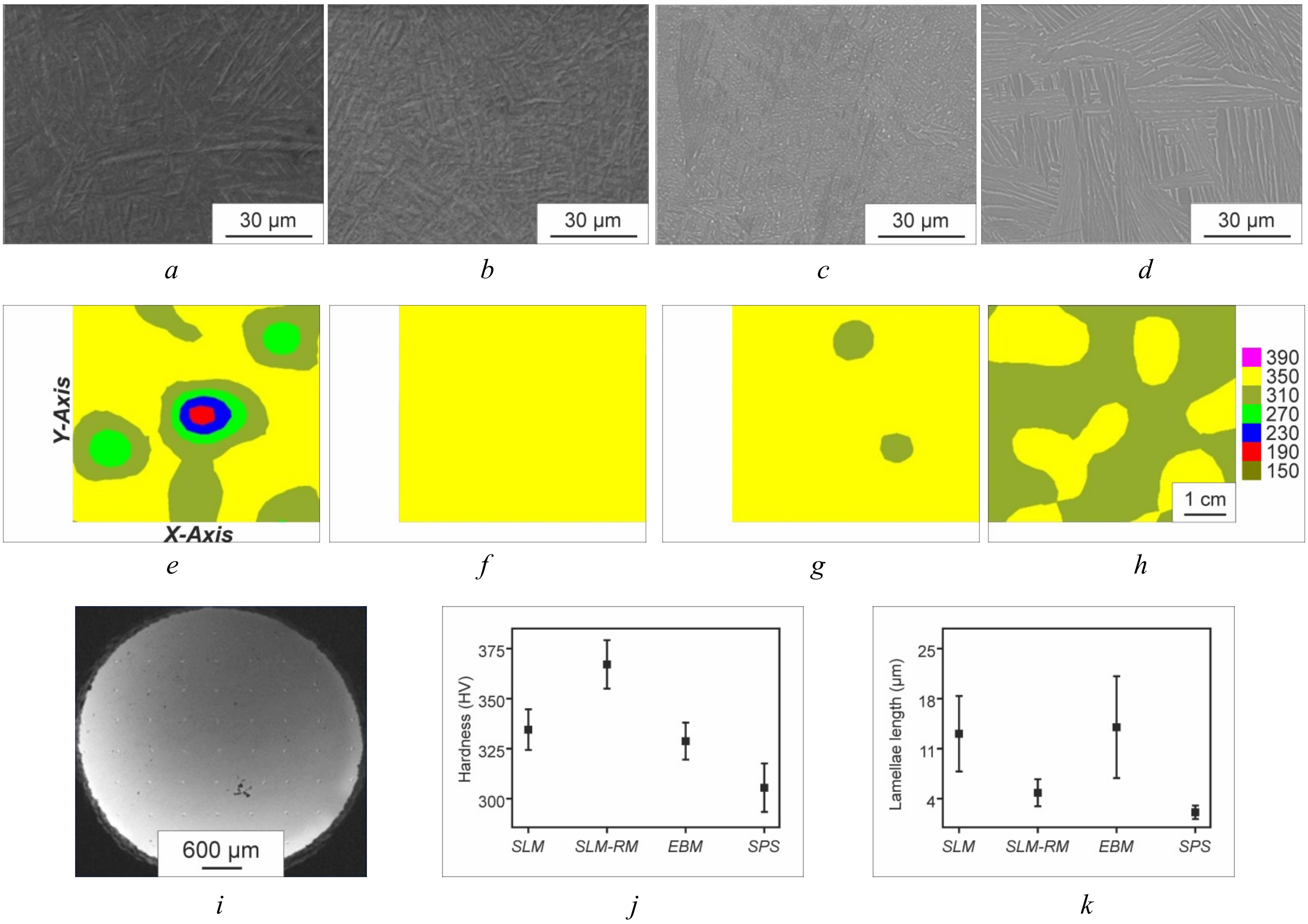

Fig. 3. SEM images of *Ti-6Al-4V* specimens fabricated using:

a – *SLM*; *b* – *SLM-RM*; *c* – *EBM*; *d* – *SPS*. Contour maps for hardness values of the samples: *e* – as-built *SLM*; *f* – *SLM-RM*; *g* – *EBM*; *h* – *SPS*; *i* – optical microscope image of hardness indentation points; *j* – comparison of *Vickers* hardness of *Ti-6Al-4V* specimens fabricated via *SLM*, *SLM-RM*, *EBM*, and *SPS*; *k* – length of lamellae in *SLM*, *SLM-RM*, *EBM*, and *SPS* samples

particularly *SLM*, is very high, and higher than that of traditional manufacturing processes. On the other hand, *SPS* has a much lower cooling rate than *AM*, and the microstructure of the *SPS* sample consists of **α** + **β** lamellae.

Based on the *SEM* observations, the lamella length in *SLM*, *SLM-RM*, *EBM*, and *SPS* samples varies; the lamella lengths were measured, and the results are shown in Fig. 3, *k*. As can be seen, the *EBM* part exhibits a smaller lamella size (Fig. 3, *k*). In addition, the hardness of the fabricated samples via *SLM*, *EBM*, and *SPS* was measured, and the results are shown in Fig. 3, *j*. It can be observed that the average *Vickers* hardness of the *SLMed* samples increased from 335 HV for as-built *SLM* to 368 HV for *SLM-RM*. The variation in hardness is probably attributed to the differences in microstructural morphology. The as-built *SLM* sample exhibited higher hardness compared to the *EBM* and *SPS* samples.

Moreover, the variation in hardness values of the fabricated *Ti-6Al-4V* samples using different processes, including *SLM*, *EBM*, and *SPS*, is illustrated in the form of contour graphs in Figs. 3, *e*–*h*. Hardness mapping has been used as a tool to quantify the heterogeneity of the samples, which is important for understanding material behavior. The hardness variation (heterogeneity) decreased, and the sample appeared to become more homogeneous with the re-melting strategy. It can also be noted that the hardness is more uniform for *EBM*.

The density and distribution of surface porosity in the parts fabricated using *SLM*, *EBM*, and *SPS* were investigated, and the mean pore size and standard deviation are illustrated in Fig. 4, *e*. The surface porosity in the *SLM* sample is mostly irregular in shape (Fig. 4, *a*). The average pore size decreased with the re-melting strategy (*SLM-RM*), and the lack-of-fusion porosity (irregular in shape) disappeared (Fig. 4, *b*). However, spherical gas porosity remained due to the presence of the protective gas atmosphere.

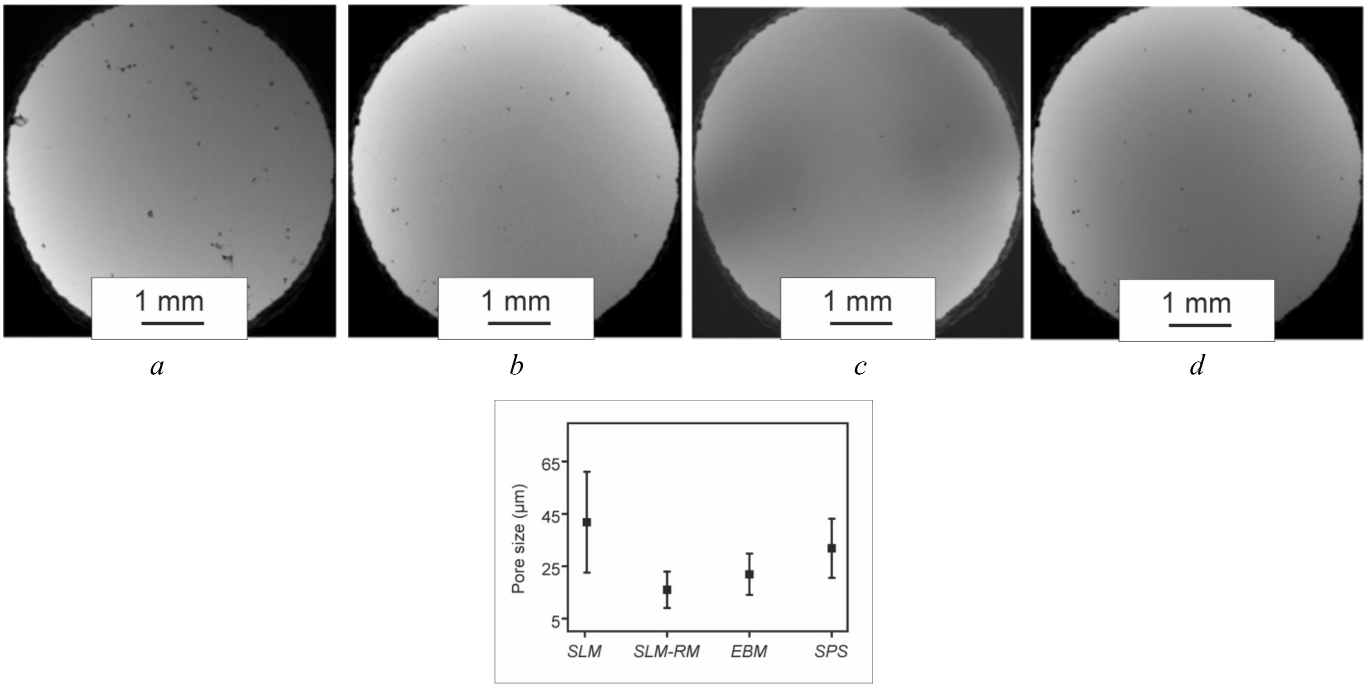

a *b* *c* *d*

e

Fig. 4. Surface porosity of parts fabricated via *SLM (a)*, *SLM-RM(b)*, *EBM(c)*, *SPS(d)*. Average pore size for samples fabricated via *SLM*, *SLM-RM*, *EBM*, and *SPS (e)*

Zhou et al. [16] prepared *TC4* alloy via *SLM* under vacuum (without a protective gas atmosphere at positive pressure) and compared the results with those obtained by conventional *SLM* (with a protective gas atmosphere). They reported that the porosity of *SLM* under vacuum was lower than that of conventional *SLM*.

It can be seen that the average pore size in the *EBM* sample (Fig. 4, *c*) is lower than that in the as-built *SLM* (Fig. 4, *a*) and *SPS* (Fig. 4, *d*) samples.

Conclusion

In this study, the microstructures and mechanical properties of *Ti-6Al-4V* parts fabricated via *EBM*, *SPS*, and *SLM* were investigated. The microstructures and mechanical properties of *Ti-6Al-4V* alloy parts manufactured by additive melting using *SLM* were compared with those of parts manufactured using a remelting strategy, as well as those produced by *EBM* and *SPS*. The microstructure of the additively manufactured samples, namely *SLM* and *EBM*, consisted of the **α/α′** phase. The sintered *Ti-6Al-4V* powder via *SPS* exhibited a dual-phase structure consisting of **α + β** phases. The hardness of the as-built *SLM* samples was higher than that of the *EBM* and *SPS* samples, with the average hardness of the as-built *SLM* specimens found to be 335 HV, increasing to 368 HV under the effect of the re-melting strategy. Additionally, the hardness variation (inhomogeneity) of *SLM* samples decreased, and the samples appeared to become more homogeneous when the re-melting strategy was applied. Surface porosity was observed in *SLM*, *EBM*, and *SPS* samples. The surface porosity of *SLM* samples was higher than that of the *EBM* and *SPS* samples. However, lack-of-fusion pores disappeared with the application of the re-melting strategy.

References

1. Murr L.E., Quinones S.A., Gaytan S.M., Lopez M.I., Rodela A., Martinez E.Y., Hernandez D.H., Martinez E., Medina F., Wicker R.B. Microstructure and mechanical behavior of Ti-6Al-4V produced by rapid-layer manufacturing, for biomedical applications. *Journal of the Mechanical Behavior of Biomedical Materials*, 2009, vol. 2, pp. 20–32. DOI: 10.1016/j.jmbbm.2008.05.004.

2. Thijs L., Verhaeghe F., Craeghs T., Humbeeck J.V., Kruth J.P. A study of the microstructural evolution during selective laser melting of Ti-6Al-4V. *Acta Materialia*, 2010, vol. 58 (9), pp. 3303–3312. DOI: 10.1016/j.actamat.2010.02.004.

3. Vilaro T., Colin C., Bartout J.D. As-fabricated and heat-treated microstructures of the Ti-6Al-4V alloy processed by selective laser melting. *Metallurgical and Materials Transactions A*, 2011, vol. 42, pp. 3190–3199. DOI: 10.1007/s11661-011-0731-y.

4. Facchini L., Magalini E., Robotti P., Molinari A., Höges S., Wissenbach K. Ductility of a Ti-6Al-4V alloy produced by selective laser melting of prealloyed powders. *Rapid Prototyping Journal*, 2010, vol. 16 (6), pp. 450–459. DOI: 10.1108/13552541011083371.

5. Karimi J., Ma P., Jia Y.D., Prashanth K.G. Linear patterning of high entropy alloy by additive manufacturing. *Manufacturing Letters*, 2020, vol. 24, pp. 9–13. DOI: 10.1016/j.mfglet.2020.03.003.

6. Karimi J., Antonov M., Prashanth K.G. Effect of wear debris entrapment on the tribological performance of AlCoCrFeNi produced by selective laser melting or spark plasma sintering. *Metallurgical and Materials Transactions A*, 2022, vol. 53, pp. 4004–4010. DOI: 10.1007/s11661-022-06805-z.

7. Karimi J., Kollo L., Prashanth K.G. Characterization of gas-atomized equiatomic AlCoCrFeNi powder for additive manufacturing. *Metallurgical and Materials Transactions A*, 2023, vol. 54, pp. 3417–3424. DOI: 10.1007/s11661-023-07129-2.

8. Karimi J., Kollo L., Prashanth K.G. Tailoring anisotropy and heterogeneity of selective laser melted Ti6Al4V alloys. *Transactions of the Indian National Academy of Engineering*, 2023, vol. 8, pp. 245–251. DOI: 10.1007/s41403-023-00393-z.

9. Karimi J., Xie M.S., Wang Z., Prashanth K.G. Influence of substructures on the selective laser melted Ti-6Al-4V alloy as a function of laser re-melting. *Journal of Manufacturing Processes*, 2021, vol. 68, pp. 1387–1394. DOI: 10.1016/j.jmapro.2021.06.059.

10. Kok Y., Tan X.P., Wang P., Nai M.L.S., Loh N.H., Liu E., Tor S.B. Anisotropy and heterogeneity of microstructure and mechanical properties in metal additive manufacturing: a critical review. *Materials & Design*, 2018, vol. 139, pp. 565–586. DOI: 10.1016/j.matdes.2017.11.021.

11. Maity T., Chawake N., Kim J.T., Eckert J., Prashanth K.G. Anisotropy in local microstructure – Does it affect the tensile properties of the SLM samples? *Manufacturing Letters*, 2018, vol. 105, pp. 33–37. DOI: 10.1016/j.mfglet.2018.02.012.

12. Yan Q., Chen B., Kang N., Lin X., Lv S., Kondoh K., Li S., Li J.S. Comparison study on microstructure and mechanical properties of Ti-6Al-4V alloys fabricated by powder-based selective-laser-melting and sintering methods. *Materials Characterization*, 2020, vol. 164, p. 110358. DOI: 10.1016/j.matchar.2020.110358.

13. Karimi J. *Microstructural homogenisation of selective laser melted Ti6Al4V and CoCrFeMnNi high-entropy alloys*. Doctoral Thesis. Tallinn University of Technology, Estonia, 2022.

14. Mercelis P., Kruth J.P. Residual stresses in selective laser sintering and selective laser melting. *Rapid Prototyping Journal*, 2006, vol. 12, pp. 254–265. DOI: 10.1108/13552540610707013.

15. Brodie E.G., Medvedev A.E., Frith J.E., Dargusch M.S., Fraser H.L., Molotnikov A. Remelt processing and microstructure of selective laser melted Ti25Ta. *Journal of Alloys and Compounds*, 2020, vol. 820, p. 153082. DOI: 10.1016/j.jallcom.2019.153082.

16. Zhou B., Zhou J., Li H., Lin F. A study of the microstructures and mechanical properties of Ti6Al4V fabricated by SLM under vacuum. *Materials Science and Engineering: A*, 2018, vol. 724, pp. 1–10. DOI: 10.1016/j.msea.2018.03.021.

17. Yang J., Yu H., Yin J., Gao M., Wang Z., Zeng X. Formation and control of martensite in Ti-6Al-4V alloy produced by selective laser melting. *Materials & Design*, 2016, vol. 108, pp. 308–318. DOI: 10.1016/j.matdes.2016.06.117.

18. Cheng X.Y., Li S.J., Murr L.E., Zhang Z.B., Hao Y.L., Yang R. Medina F., Wicker R.B. Compression deformation behavior of Ti-6Al-4V alloy with cellular structures fabricated by electron beam melting. *Journal of the Mechanical Behavior of Biomedical Materials*, 2012, vol. 16, pp. 153–162. DOI: 10.1016/j.jmbbm.2012.10.005.

19. Karimi J., Bohlen A., Kamboj N., Seefeld T. Automated determination of grain features for wire arc additive manufacturing. *Journal of Materials Engineering and Performance*, 2023, vol. 32, pp. 10402–10411. DOI: 10.1007/s11665-023-08266-w.

20. Ahmed T., Rack H.J. Phase transformations during cooling in α+β titanium alloys. *Materials Science and Engineering: A*, 1998, vol. 243, pp. 206–211. DOI: 10.1016/S0921-5093(97)00802-2.

Conflicts of Interest

The author declares no conflict of interest.